CHALMERS
UNIVERSITY OF TECHNOLOGY

Preparation and Characterization of TEMPO-CNFs/Cellulose Acetate$_{DS=0.9}$ Composite Films

An Investigation into New Biobased Composites

Master's thesis in Materials Chemistry

Hongrun Chen

DEPARTMENT OF CHEMISTRY AND CHEMICAL ENGINEERING

CHALMERS UNIVERSITY OF TECHNOLOGY
Gothenburg, Sweden 2024
www.chalmers.se

Master's thesis 2024

Preparation and Characterization of TEMPO-CNFs/Cellulose Acetate$_{DS=0.9}$ Composite Films

An Investigation into New Biobased Composites

HONGRUN CHEN

CHALMERS
UNIVERSITY OF TECHNOLOGY

Department of Chemistry and Chemical Engineering
Division of Organic Chemistry
Chalmers University of Technology
Gothenburg, Sweden 2024

Preparation and Characterization of TEMPO-CNFs/Cellulose Acetate$_{DS=0.9}$ Composite Films
An Investigation into New Biobased Composites
Hongrun Chen

Supervisor: Akira Isogai, University of Tokyo
Examiner: Gunnar Westman, Department of Chemistry and Chemical Engineering

Master's Thesis 2024
Department of Chemistry and Chemical Engineering
Division of Organic Chemistry
Chalmers University of Technology
SE-412 96 Gothenburg
Telephone +46 31 772 1000

Cover: A transparent composite film made from TEMPO-oxidized cellulose nanofibril with carboxyl group and cellulose acetate$_{DS=0.9}$.

Typeset in LaTeX
Printed by Chalmers Reproservice
Gothenburg, Sweden 2024

Preparation and Characterization of TEMPO-CNFs/Cellulose Acetate$_{DS=0.9}$ Composite Films
An Investigation into New Biobased Composites
HONGRUN CHEN
Department of Chemistry and Chemical Engineering
Chalmers University of Technology

Abstract

New biobased composite films were prepared using water-soluble cellulose acetate, with a degree of substitution (DS) of 0.9 as a polymer matrix, reinforced with two types of TEMPO-oxidized cellulose nanofibrils (TEMPO-CNFs) separately: one with carboxylate groups (-COONa) and one with carboxyl groups (-COOH). The TEMPO-CNF-COOH was obtained by protonation of TEMPO-CNF-COONa using HCl at pH 2.0. The composite films were prepared using a water system casting and drying method. The composite films were designed to contain 0-16% TEMPO-CNFs, each exhibiting high light transparencies. However, the composite films with low concentrations of TEMPO-CNFs exhibited high haze values, possibly due to the height differences caused by individual CNFs on the surface. The composite films showed enhanced tensile strength and Young's modulus with increasing TEMPO-CNF concentrations. This is reasonable due to the superior mechanical property provided by TEMPO-CNFs. The change from TEMPO-CNF-COONa to TEMPO-CNF-COOH further improved their mechanical properties, indicating a stronger composite film structure. X-ray diffraction (XRD) patterns of the films showed an increasing crystallinity with increasing TEMPO-CNF contents. Transmission electron microscopy (TEM) images confirmed a homogeneous distribution of TEMPO-CNFs within the film, providing the composite films with reasonable mechanical properties.

Keywords: biobased composites, TEMPO-oxidized cellulose nanofibrils, TEMPO-CNF-COONa, TEMPO-CNF-COOH, cellulose acetate$_{DS=0.9}$, casting and drying.

Acknowledgements

Firstly, I would like to express my gratitude to my supervisor, Prof. Akira Isogai, at Tokyo University for providing me with the opportunity to work in his lab and on this project. I am also thankful to PhD students Gaoyuan Hou and Korawit Chibanyoung for their patient help and guidance during my time at the University of Tokyo. Special thanks to Dr. Miyuki Takeuchi for her guidance and assistance with performing the transmission electron microscopy.

I would also like to thank Prof. Tsuguyuki Saito and Prof. Shuji Fujisawa at the Laboratory of Bionanomaterials and Cellulose Sciences at the University of Tokyo for allowing me to use their analytical instruments for my project.

Lastly, I am grateful to my examiner, Gunnar Westman, for introducing Prof. Akira Isogai to me and making my dream of studying in Japan become a reality.

Hongrun Chen, Gothenburg, August 2024

List of Acronyms

Below is the list of acronyms that have been used throughout this thesis listed in alphabetical order:

ATR	Attenuated Total Reflection
CA	Cellulose Acetate
CNC	Cellulose Nanocrystal
CNF	Cellulose Nanofibril
CNNeW	cellulose Nanonetworks
DPv	Viscosity Average Degree of Polymerization
DS	Degree of Substitution
FT-IR	Fourier Transform Infrared
R.H.	Relative Humidity
TEM	Transmission Electron Microscopy
TEMPO	2,2,6,6-Tetramethylpiperidinyl-1-oxyl
TEMPO-CNF	TEMPO-Oxidized Cellulose Nanofibril
TEMPO-CNF-COONa	TEMPO-CNF with Sodium Carboxylate Groups
TEMPO-CNF-COOH	TEMPO-CNF with Carboxyl Groups
TMA	Thermomechanical Analysis
UV-VIS	Ultraviolet-Visible
XRD	X-ray Diffraction

Nomenclature

Below is the nomenclature of parameters and variables that have been used throughout this thesis.

Parameters

T_3	Instrument diffusion
T_4	Sample diffusion
T_d	Diffuse Transmittance
T_t	Total light transmittance
λ	Wavelength of the X-rays
d	Spacing between crystal planes

Variables

n	Order of the diffraction peak
θ	Angle of incidence of the X-rays

Contents

List of Figures

1

Introduction

Today, the applications of conventional synthetic polymers in various areas have provided huge convenience and advancement to our society [1]. On the other hand, the low degradation rate and accumulation of synthetic polymer materials have created serious problems for the environment. As a result, the search for new alternative materials has become a focus in recent years. One solution is to utilize renewable and biodegradable materials such as cellulose.

Cellulose is a biopolymer composed of repeating $\beta(1\rightarrow4)$ linked D-glucose units. It makes up approximately 50% of terrestrial plant cell walls, making it the most abundant biopolymer on the planet [2]. Currently, a significant focus has been placed on producing materials from cellulose and cellulose derivates due to their sustainability and biodegradability. With the development of efficient utilization of cellulosic materials, they have a high potential to become a source of sustainable materials for advanced materials, medical and personal care fields, the food industry, and etc.

One category of materials that can be refined from cellulose is nanocellulose, which is defined as fibers with a width $<$100 nm [2, 3]. Currently, three types of nanocellulose have been found: cellulose nanonetworks (CNNeWs), cellulose nanofibrils (CNFs), or cellulose nanocrystals (CNCs). In this project, the focus will only be on CNFs.

CNFs are fibrillar materials containing nanoscale cellulose fibrils. It has lengths $>$500 nm and widths of homogeneous $\approx$3 nm [2, 3]. They are dispersed in water without forming any fibril bundles. Several methods of preparing the CNFs have been established, one popular method is chemical pretreatment using 2,2,6,6-tetramethylpiperidine-1-oxyl radical (TEMPO). This is an oxidation process that converts the C6-hydroxyl groups to C6-carboxylate groups.

Another important material that can be derived from cellulose is cellulose acetate (CA), produced by the acetylation of cellulose [4]. It is one of the most common derivatives of cellulose and is currently widely used in the industry for film, membranes, fibers, etc. CA offers several advantages in physical properties such as excellent optical clarity, biodegradability, and high toughness. Generally, CA refers to CA with a degree of substitution (DS) equal to 2.5 [4]. However, the degree of substitution can be controlled by an additional hydrolysis process, making it possible to produce CA with a lower DS value [5, 6].

In this project, new composites was prepared by incorporating $\mathrm{CA}_{DS=0.9}$ as the polymer matrix with each of the two different types of TEMPO-oxidized CNFs

(TEMPO-CNFs) separately as the reinforcement materials.

1.1 Background

This master's thesis was conducted at the University of Tokyo under the guidance of Prof. Akira Isogai and his team. The idea for this project was provided by Prof. Isogai, who is currently a Special Professor at the University of Tokyo and is a world-leading scientist in the field of cellulose and nanocellulose materials. Prof. Isogai and his team at the University of Tokyo have led several fundamental and application studies on CNFs. In fact, his team was the first to successfully prepare completely individualized CNFs with homogeneous widths of approximately ≈3 nm from plant cellulose fibers using chemical pretreatments.

1.2 Aim

This project aims to prepare and characterize new composites using $CA_{DS=0.9}$ as the polymer matrix with each of the two different types of TEMPO-oxidized CNFs (TEMPO-CNFs) separately as the reinforcement materials. The TEMPO-CNFs to be used are TEMPO-CNF with carboxylate groups (TEMPO-CNF-COONa) and with carboxyl groups (TEMPO-CNF-COOH), with the latter prepared through protonation of the former. The hypothesis is that TEMPO-CNF-COOH will form more hydrogen bonds with the OH-group on $CA_{DS=0.9}$, thereby further enhancing the mechanical properties.

2

Theory

2.1 Cellulose Nanofibrils

As mentioned earlier, CNFs are fibrillar materials containing nanoscale cellulose fibrils, with widths of homogeneous ≈3 nm and lengths >500 nm [2, 3]. They are dispersed in water individually without forming any fibril bundles. Conventional CNFs are prepared from the mechanical integration of cellulose microfibrils in the water. Cellulose microfibrils are the naturally formed smallest element next to the cellulose molecules with ≈3 nm in width and several micrometers in length, Fig. 2.1. However, the conventional method is highly energy-consuming due to the strong intermolecular forces between cellulose microfibrils. Moreover, with conventional mechanical integration, the produced CNFs will show inhomogeneous morphologies and properties. Therefore, a more efficient method is needed for the commercial production of CNFs.

One way to overcome the problems of the conventional method is to add a chemical pretreatment before the mechanical disintegration [2]. During chemical pretreatment, cellulose microfibrils will obtain highly anionic charges on their surface, which in turn creates osmotic effects and electrostatic repulsion between them. This weakens the interfibrillar hydrogen bonds between cellulose microfibrils so that they can be separated through gently mechanical disintegration in water, forming individualized CNFs in water.

TEMPO-oxidation using TEMPO is a well-established chemical pretreatment for preparing CNFs [2, 3]. The cellulose microfibrils are subjected to treatment with

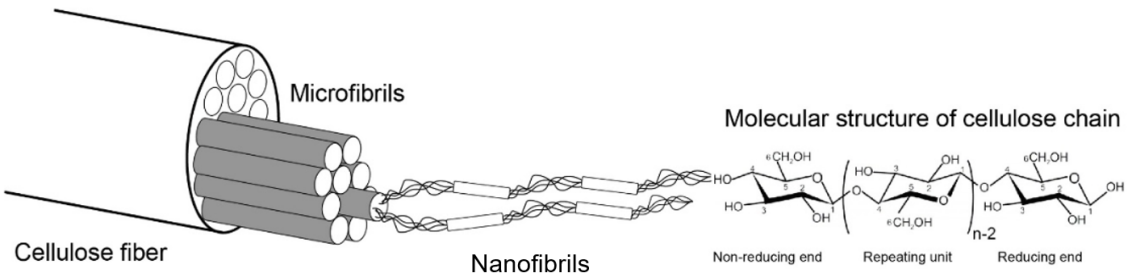

Figure 2.1: Hierarchical structure of cellulose fiber showing molecular structure [7]. Figure reinterpreted from Zambrano et al. 2020.

TEMPO, NaBr, and NaClO in water with a pH of 10. During this process, the C6-hydroxyl group on the surface of the cellulose microfibril is almost completely converted to sodium C6-carboxylate groups, Fig. 2.2. These sodium C6-carboxylate groups, in turn, result in electrostatic repulsion between cellulose microfibrils. By mechanical disintegration, the TEMPO-oxidized cellulose microfibrils can be easily separated.

Aside from TEMPO oxidation, CNFs can undergo various chemical pretreatments to introduce other charge groups on the surfaces [2, 3]. This will provide the material with new and functional properties such as hydrophobic, catalytic, gas-separation properties, etc.

However, to commercialize CNFs, further studies are required to accumulate more fundamental data. One example of a technical issue that needs to be overcome is the water removal process of nanocellulose dispersions, which requires more research [2].

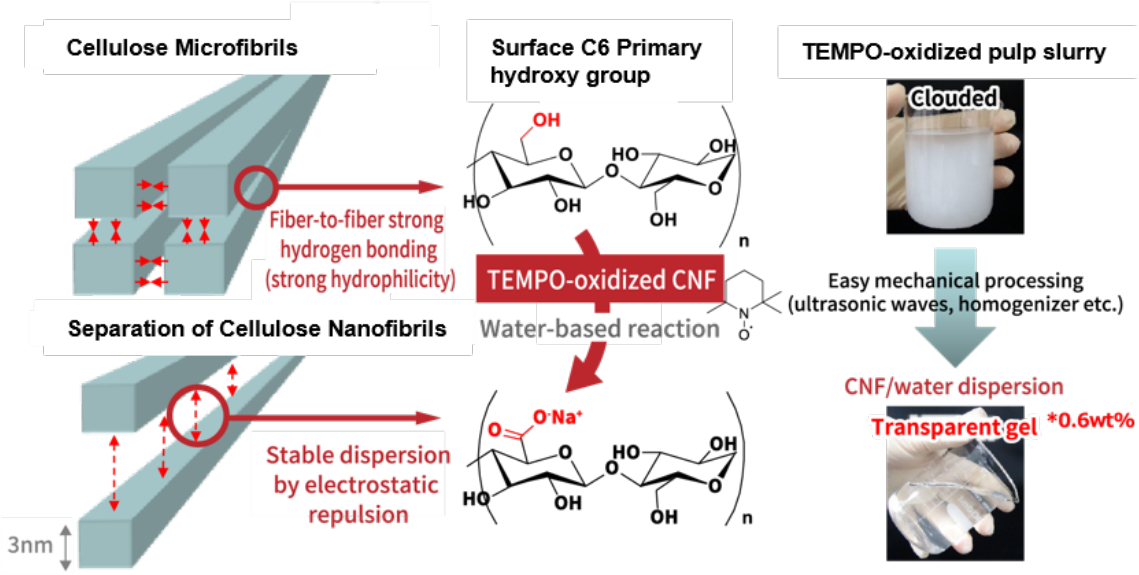

Figure 2.2: The process of separating cellulose microfibrils through TEMPO-oxidation [8]. Figure reinterpreted from Kao Corporation.

2.2 Cellulose Acetate

CA is produced by acetylation of cellulose [9, 10]. In the acetylation process, cellulose is dissolved in the acetic acid, and an excessive acetic anhydride is added in the presence of sulfuric acid as a catalyst. An excess acetic anhydride is to ensure that all of the hydroxyl groups on cellulose are acetylated. After fully acetylation, it is subject to a hydrolysis process which makes it possible to control the DS-value of the fully acetylated cellulose acetate.

In general, commercial CA usually refers to CA with a DS value around 2.5 as it has a good solubility to most common solvents. However, with the hydrolysis process, a

lower DS-value of CA can be produced. CA with DS-values around 1 are quite new materials with only a small amount of investigation being conducted. Therefore, to accurately ascertain the suitable use of CA with DS-values around 1, more research needs to be conducted.

The previous article reported that CA with lower DS-values is more biodegradable and has higher crystallinity [5]. The CA with DS-values close to 1 are water-soluble.

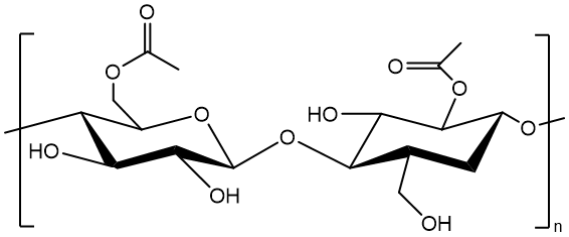

Figure 2.3: Cellulose acetate with a degree of substitution equal to 1.

2.3 Composite

A polymer composite is a material made by combining two or more distinct components to create a new material with improved properties [1]. A polymer composite is at least consisted with of two components: a polymer matrix and a reinforcement material.

The polymer matrix is a continuous phase in the composite and holds the composite together. It can be either thermosetting or thermoplastic material [1]. On the other hand, the reinforcement material is dispersed inside the polymer matrix to provide specific properties or enhance the desired properties. It can consist of different forms such as fiber, particular fillers, nanoparticles, and etc. These components together provide the composite material with enhanced properties compared to the individual component itself.

The advantage of using TEMPO-CNFs as a reinforcement material is their ability to enhance the mechanical properties without sacrificing the transparency of the polymer matrix [2, 11, 12]. Moreover, TEMPO-CNFs have high strength, stiffness, and are lightweight, which benefits the properties of the composite. Additionally, they have a high aspect ratio, forming a strong network inside the composite and enhancing the load transfer compared to other polymers. Therefore, TEMPO-CNFs is possible provide the polymer matrix with high load transfer and enhanced mechanical properties while achieving a lower weight compared to other reinforcement materials.

2.4 Tensile Test

A tensile test is a fundamental method used to determine the mechanical properties of materials under controlled tension [13]. It involves applying a controlled pulling

force from both sides of a specimen until it breaks. The key parameters measured in a tensile test are stress, strain, and Young's modulus.

2.5 Fourier Transform Infrared Spectroscopy

Fourier Transform Infrared (FT-IR) Spectroscopy is an analytic tool used to obtain an infrared spectrum of absorption or emission of a sample [14]. FT-IR spectrometers are widely used in chemical analysis and materials science to identify chemical compounds and study molecular structures.

The basic principle is an instrument that emit IR radiation containing many different frequencies of light. The sample will absorb the emitted radiation and cause distinctive changes in the vibrations and rotations of the molecular bonds [14]. The absorption of the radiation will be analyzed by the instrument and the chemical structure of the sample can be identified.

In this project, attenuated total reflectance (ATR) of FT-IR was used to analyze the sample [14]. It is a low-penetration method that measures the surface of the material by direct contact with ATR attachment.

2.6 Ultraviolet-Visible Spectrometer

Ultraviolet-visible (UV-VIS) spectrometer is an analytic instrument to measure the absorption or transmission of ultraviolet and visible light through a sample [14]. This is a common method to determine the optical properties of materials.

The basic principle involves shooting monochromatic light beams with different wavelengths into a sample and measuring the amount of light that passes through the sample at each wavelength [14]. The transmission of the light can be calculated as the amount of light passing through the sample divided by the amount of light emitted from the instrument.

During the measurement, the total light transmittance (the total amount of light passing through the sample, denoted as T_t), the sample diffusion (the total amount of light that is scattered by the sample, denoted as T_4), and the instrument diffusion (the total amount of light that is scattered by the instrument, denoted as T_3) could be measured, as shown in Fig. 2.4 [15].

With these parameters, the haze value of the material can be calculated using the following equations:

$$T_d = T_4 - T_3(\frac{T_t}{100}) \tag{2.1}$$

$$Haze = (\frac{T_d}{T_t}) \tag{2.2}$$

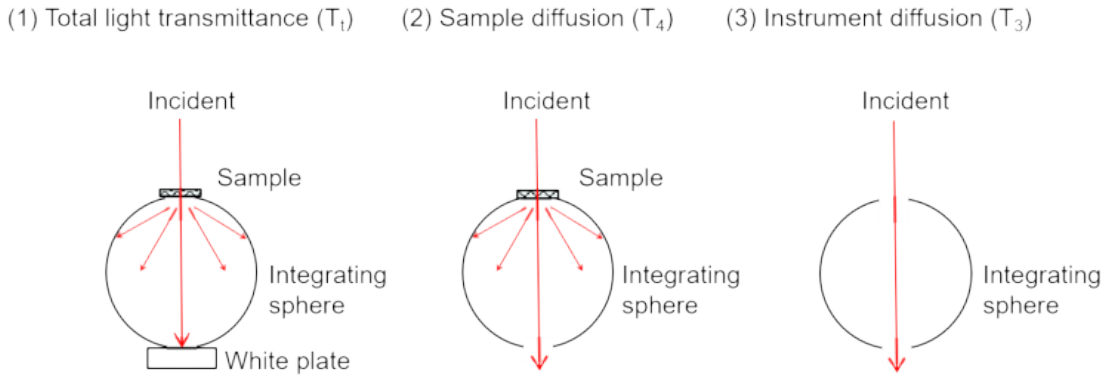

Figure 2.4: Haze value measurement [15].

2.7 Thermomechanical Analysis

Thermomechanical analysis (TMA) is a measurement tool used to detect the dimensional changes of a sample during the evaluated temperature while it is subjected to controlled mechanical stress or strain [16]. This method is commonly used for measuring thermal properties such as thermal expansion of the materials.

2.8 X-ray Diffraction

X-ray diffraction (XRD) is an analytic tool used to analyze the sample's composition and crystal structure [17]. It is based on analyzing the diffraction of the X-ray caused by the interaction between the X-rays and the atoms inside a crystalline material.

In the XRD instrument, X-rays with specific wavelengths are emitted to the sample [17]. The X-ray will interact with the electrons in the atoms and cause diffraction of X-rays. The diffracted X-rays can analyzed by the detector using Bragg's law:

$$n * \lambda = 2 * d * sin\theta \tag{2.3}$$

where θ stands for the incidence angle of the X-rays, (d) stands for the spacing between crystal planes, and (λ) for the wavelength of the X-rays [17]. When X-rays are diffracted by a crystalline material, they form a diffraction pattern consisting of peaks at specific angles. Each peak corresponds to a set of crystal planes within the material that diffracted the X-rays.

2.9 Transmission Electron Microscopy

Transmission Electron Microscopy (TEM) is a powerful imaging tool that uses electrons to visualize the structure of materials at a very high resolution [18].

The working principle of the TEM involves the emission of a beam of electrons. These electrons are accelerated by high voltage, which enables better penetration

and resolution in the sample [18]. When the electron beam passes through the sample, it will interact with the sample, causing elastic scattering, inelastic scattering, and diffraction.

However, only the electrons that pass through the sample without being scattered form the transmitted electron beam [18]. This transmitted electron beam carries information about the sample's structure. The intensity of the transmitted beam is detected and used to form the image.

3

Methods

3.1 Materials

A commercial TEMPO-CNF-COONa/water gel, prepared from softwood bleached kraft pulp, was provided by Nippon Paper Industries Co., Ltd., Japan. The gel-like consistency was due to the high solid content of the commercial TEMPO-CNF-COONa/water gel, ≈3 (w/w) %. A commercial $CA_{DS=0.9}$ was provided by Daicel Corporation, Japan. It had a viscosity average degree of polymerization (DPv) of 131.

3.2 Preparation of TEMPO-CNF Dispersions and Cellulose Acetate Solution

The commercial TEMPO-CNF-COONa/water gel was diluted to a 0.5% (w/w) TEMPO-CNF-COONa/water dispersion. Some large clusters were observed after filtration, therefore, an additional vacuum filtration step was added to the process. The $CA_{DS=0.9}$ powder was dissolved in water and then filtered to remove undissolved particles, obtaining a 3% (w/w) cellulose acetate solution in water. A complete scheme for the preparation of the composite films is shown in Fig. 3.1.

A TEMPO-CNF-COOH dispersion was prepared by protonating commercial TEMPO-CNF-COONa using 1% HCl. To achieve this, 1% HCl was slowly added to a 0.5% (w/w) TEMPO-CNF-COONa/water dispersion while stirring with a magnetic stirrer, setting the pH to approximately 2.0. The dispersion was then stirred for 30 minutes at room temperature, causing the dispersion to form small gel particles. The gel-like dispersion was washed with deionized water at 9000 rpm/g for 10 min, repeated four times, until the pH of the washing water became neutral. The resulting gel after washing was dispersed in water and passed through a high-pressure homogenizer, NanoVater NVC-ES008A-D10, four times to obtain a flowable dispersion.

3.3 Preparation of the Composite Film

The composite films were prepared using the simple casting and drying method. A 0.5% (w/w) TEMPO-CNF dispersion and a 3% (w/w) $CA_{DS=0.9}$ were stirred

with a magnetic stirrer at room temperature for 2 hours to achieve a homogeneous mixture. Air bubbles inside the aqueous mixture were removed using a Thinky AR-100, rotating at 2200 rpm for 3 minutes, repeated twice. The mixture was then poured into a polyethylene petri dish and dried in an oven at 40°C and 80% relative humidity (R.H.) for at least 24 hours. The dried film was peeled from the petri dish and conditioned at 23°C and 80% R.H. for at least 1 day before use. Five different composite films with different concentrations of each TEMPO-CNFs were prepared: 0%, 2%, 4%, 8%, and 16%.

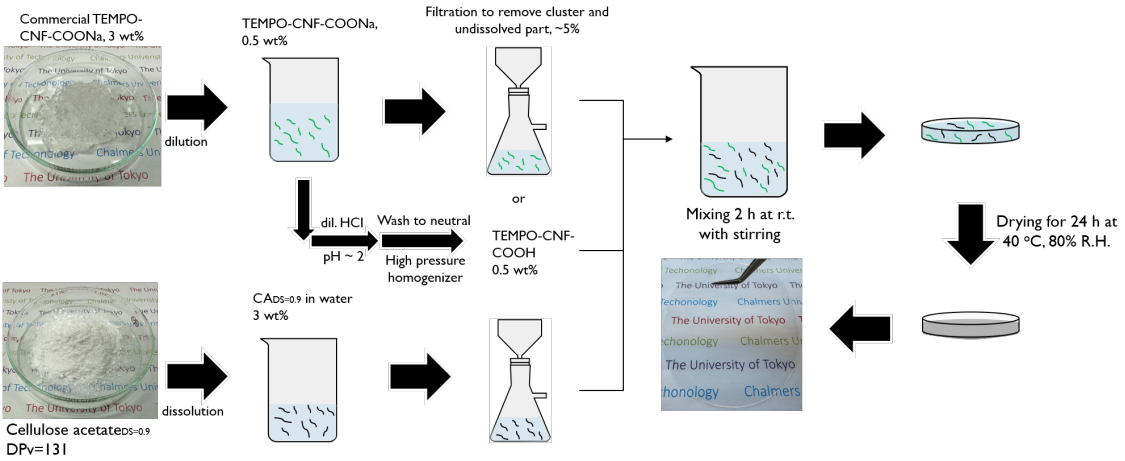

Figure 3.1: A scheme for the preparation of the composite films.

3.4 Analysis

3.4.1 Densities and Moisture Contents

The densities of the films were determined by measure five different points of the films and calculating the average values. The moisture contents of the films were measured by drying the films at 105°C for 3 hours.

3.4.2 Fourier Transform Infrared Spectroscopy

The conversion from TEMPO-CNF-COONa to TEMPO-CNF-COOH was ascertained using FT-IR spectra of the TEMPO-CNF-COONa and TEMPO-CNF-COOH films. A Jasco FT/IR-6100 spectrometer was used under transmission mode, scanning from 600 to 4000 cm^{-1} with a 4 cm^{-1} resolution. The films were dried at 105°C for 1 hour before analysis.

3.4.3 Ultraviolet-Visible Spectrometer

The light transmittances of the films were measured using a JASCO V-670 ultraviolet-visible light spectrophotometer, which has a wavelength range from 300 to 800 nm. The light transmittances were normalized to a thickness of 40 µm using the Beer-Lambert law.

3.4.4 The Surface of the Composite Films

Optical microscopy, Evident Corporation SZX2-ILLTS, was used to observe the surface of the films to determine the roughness of the surface. The light from the optical microscope was directed at an oblique angle to the film's surface.

3.4.5 Tensile Test

The tensile properties of the films were evaluated using a Shimadzu EZ-SX tensile tester equipped with a 500 N load cell, operating at a 10 mm span length and a 0.5 mm/min speed. The film strips used in the tensile test were 2 mm in width and 30 mm in length. Each of them was conditioned at 23°C and 50% relative humidity for at least 24 hours before use. At least five valid data were collected for each sample.

3.4.6 X-ray Diffraction

XRD patterns were obtained using the Rigaku MiniFlex 600 X-ray diffractometer (Tokyo, Japan) operating at 40 kV and 15 mA. The set angles were from 5° to 45° with a step size of 0.05° and a scan speed of 5.0°/min.

3.4.7 Transmission Electron Microscopy

TEM images were obtained using a JEM-1400 Plus at 100 kV. The samples were prepared by hydration with 50% ethanol in water to increase the thickness of the sample. Then the hydrated samples were immersed in ethanol-water mixtures with a gradually increased concentration of ethanol until 100%. This step replaced the water in the sample with ethanol while maintaining the samples' thickness. The thickened samples were embedded in epoxy resin and ultrathin-sectioned using an Ultramicrotome (Ultracut-UTC, Leica, Germany). The cut samples were then stained with 4% aqueous uranyl acetate and Reynold's lead citrate solution.

3.4.8 Termomechanical Analysis

The thermal expansion of the composite films was measured using a Shimadzu TMA-60. Before the measurements, the samples were dried at 102°C under a nitrogen flux for 30 minutes. The thermal expansion was recorded from 30°C to 100°C at a heating rate of 5°C/min under a nitrogen atmosphere and with a 0.03 N load.

4

Results

4.1 Preparation of TEMPO-CNF Dispersions and $CA_{DS=0.9}$ Solution

After the vacuum filtration of TEMPO-CNF-COONa and $CA_{DS=0.9}$, the filtrates were $\leq$ 5%. However, for the preparation of TEMPO-CNF-COOH, the original TEMPO-CNF-COONa was not subjected to any vacuum filtration. This is because the high-pressure homogenization in the later process will fibrillate the clusters. Therefore, the clusters presented before protonation using HCl would not affect the result.

The TEMPO-CNF-COOH/water dispersion was prepared from the TEMPO-CNF-COONa/water dispersion through protonation with 1% HCl at pH ≈2.0. The dispersion formed small gel particles, which increased its viscosity and reduced its flowability. However, after disintegration with water in a high-pressure homogenizer, the dispersion became more flowable, and its viscosity decreased. The yield for the conversion from TEMPO-CNF-COONa to TEMPO-CNF-COOH is 82%.

The FT-IR spectra of TEMPO-CNF-COONa and TEMPO-CNF-COOH films were recorded in Fig. 4.1. In the figure, the characteristic peak of -COONa at 1600 cm^{-1} shifted to 1720 cm^{-1}, indicating a successful conversion from -COONa to -COOH [11]. Additionally, the spectrum of the TEMPO-CNF-COOH film no longer show the absorption band at 1400 cm^{-1}, which is characteristic of the C-O symmetric stretching of dissociated carboxyl groups.

The peak observed around 3300 cm^{-1} indicates the stretching vibration of O-H peaks [20, 21]. This peak was a result of the intra- and intermolecular H-bonds as well as the absorbed water. The peak observed at 2900 cm^{-1} indicated stretching CH_2 vibrations of the TEMPO-CNFs. The broad peaks between 900-1250 cm^{-1} indicates the backbone of the cellulose.

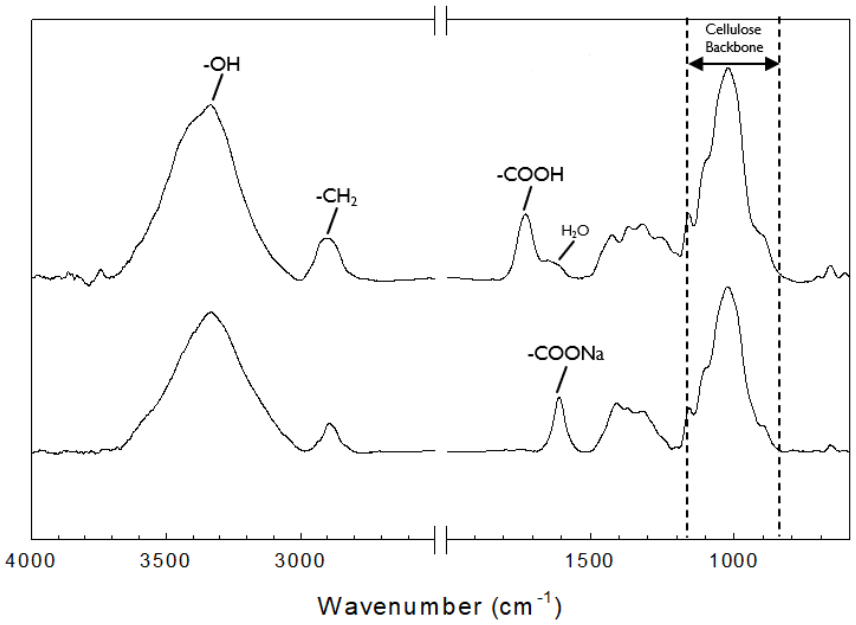

Figure 4.1: FT-IR spectra for pure TEMPO-CNF-COONa and TEMPO-CNF-COOH films.

4.2 Fundamental Properties of the Composite Films

In Fig. 4.2, the appearances of all the films are shown. Visually, all the films exhibit high transparency and clarity. However, on the 2% TEMPO-CNF-COONa composite film, some roughness at the surface is apparent. This roughness decreases with an increase in TEMPO-CNF-COONa concentration.

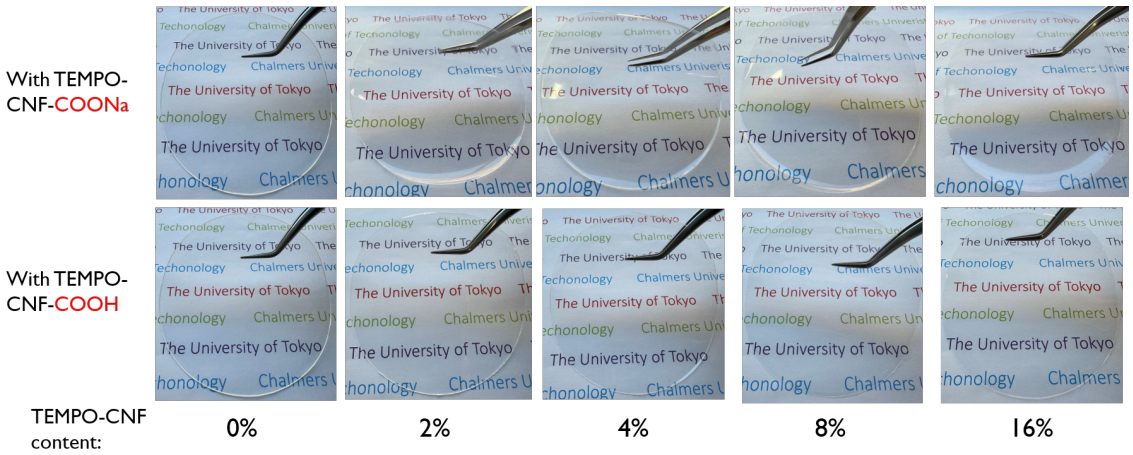

Figure 4.2: Apperance of the films.

The densities and moisture contents are shown in Fig. 4.3. The densities decrease with increasing TEMPO-CNF content, indicating the formation of pores with increasing TEMPO-CNFs. This is due to the high aspect ratios and large surface

area of TEMPO-CNF, trapping more water into the composite matrix. Therefore, the water leaves pores inside the composite after the drying process and decrease their densities. Overall, the moisture content of the films increases with increasing TEMPO-CNF concentration. However, in the case of the 2% and 4% TEMPO-CNF-COOH composite films, the moisture content shows a decreasing trend. This behavior may be due to the low concentration of TEMPO-CNF-COOH, which strengthens the structure and increases its hydrophobicity. However, with a higher concentration of TEMPO-CNF-COOH, the water absorption overcomes the hydrophobicity.

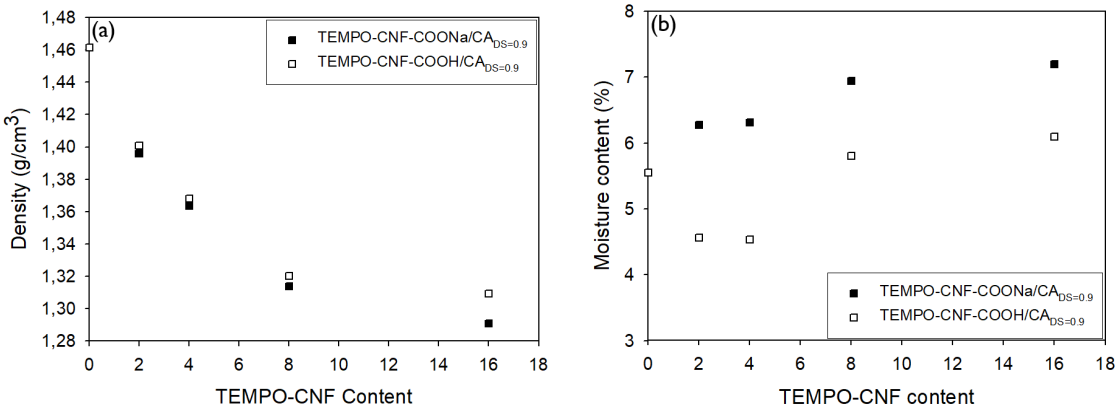

Figure 4.3: The densities and moisture contents of the composite films. a: Densities, b: Moisture contents.

4.3 Optical Properties of the Composite Films

In Fig. 4.4, the films' light transmittance and haze values are shown. All films exhibit high light transmittance, around 93% at 600 nm. Thus, it can be ascertained that the high light transparency of $CA_{DS=0.9}$ was not affected by the concentration of the TEMPO-CNFs. Among all the films, the pure $CA_{DS=0.9}$ film exhibits the lowest haze value. Whereas, the 2% composite films of both TEMPO-CNFs showed the highest haze values, then decreased with increasing TEMPO-CNF content. This is a weird phenomenon, as the haze value usually increases with increasing TEMPO-CNFs content.

To investigate this phenomenon, the surface of the 2% and 16% composite films of both TEMPO-CNFs was examined using optical microscopy, as shown in Fig. 4.5. For TEMPO-CNF-COONa composite films, the 2% composite film has a rough surface. However, the roughness decreased significantly when the content of TEMPO-CNF increased to 16%. On the other hand, in the case of TEMPO-CNF-COOH composite films, both the 2% and 16% films exhibit a smooth surface compared to TEMPO-CNF-COONa composite films. Therefore, the microscopy level surface roughness is not the main reason for the high haze of the 2% composite films.

A possible explanation for the high haze values could be the presence of height differences caused by individual TEMPO-CNFs on the composite film surfaces, as

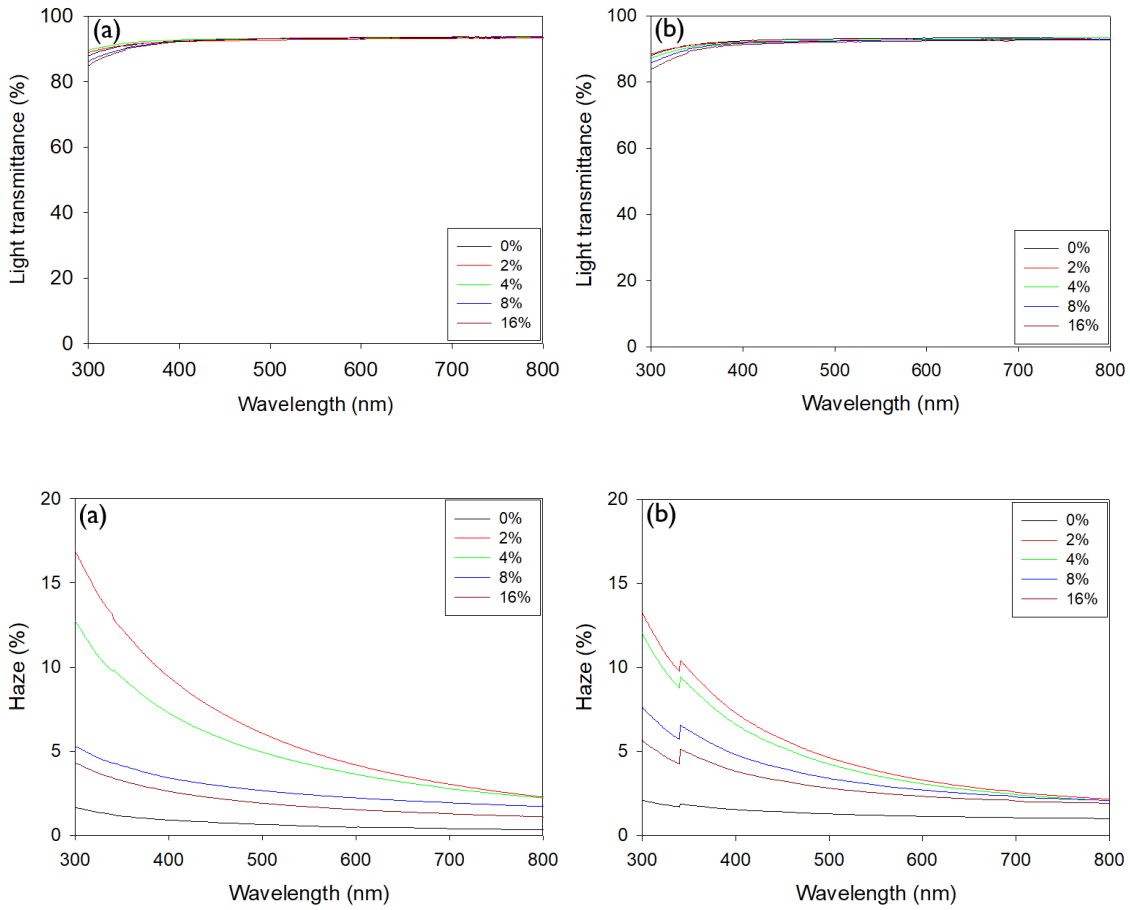

Figure 4.4: The light transmittance and haze values of the composite films. a: TEMPO-CNF-COONa, b: TEMPO-CNF-COOH.

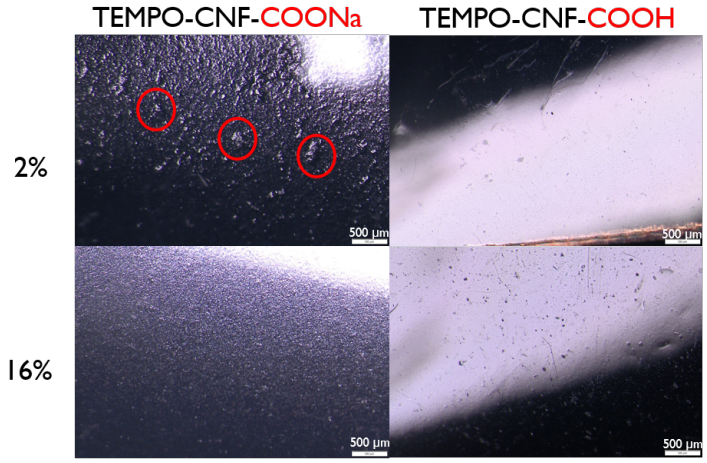

Figure 4.5: The surfaces of the composite films observed using optical microscopy.

shown in Fig. 4.6. Each bump in the figure represents an individual TEMPO-CNF on the $CA_{DS=0.9}$ surface, with an approximate width of ≈3 nm. In the 2%

composite films, the low concentration of TEMPO-CNFs results in few bumps on the surface, creating a height difference between the bumps and the $CA_{DS=0.9}$ surface. Conversely, the 16% composite films exhibit a smoother surface due to a higher amount of bumps. This behavior could explain the high haze values observed in the 2% composite films. However, the height differences caused by the TEMPO-CNFs are at the nanoscale, making them undetectable using optical microscopy.

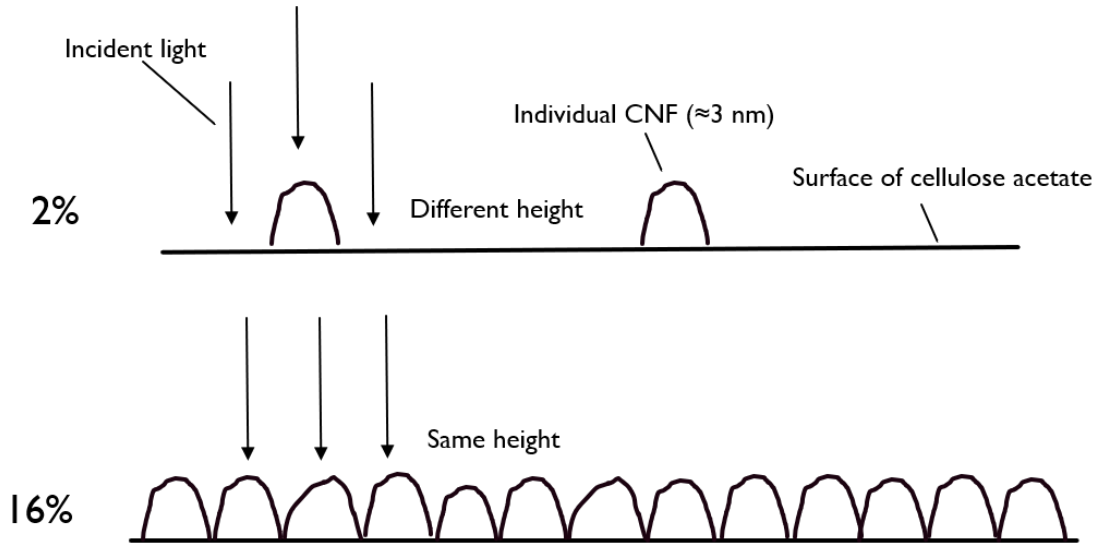

Figure 4.6: A possible mechanism for the high haze value at low concentrations of TEMPO-CNFs.

4.4 Mechanical properties of the Composite Films

The stress-strain curves of the composite films are presented in Fig. 4.7. The tensile strengths of the composite films showed a significant increase with increasing TEMPO-CNF content. Moreover, the TEMPO-CNF-COOH composite films have significantly higher tensile strength compared to the TEMPO-CNF-COONa composite films, indicating that more hydrogen bonds were formed between TEMPO-CNF-COOH and the OH group in $CA_{DS=0.9}$, providing the film with a stronger structure. The strains of the composite films showed a decreasing trend, which corresponds to the effect of TEMPO-CNFs that provide higher stiffness to the composite films.

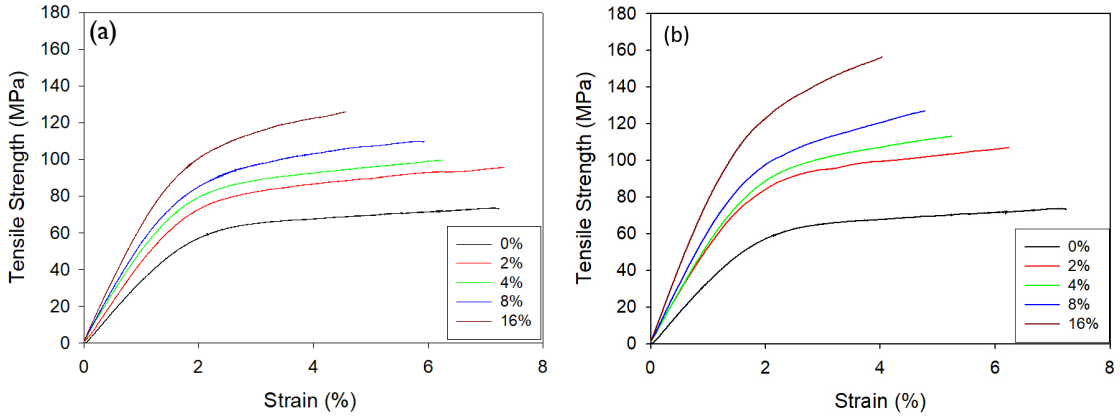

Figure 4.7: The stress-strain curves of the composite films. a: TEMPO-CNF-COONa, b: TEMPO-CNF-COOH.

The tensile properties are plotted against TEMPO-CNF contents in Fig. 4.8. The tensile strengths and Young's modulus showed significant increases with higher content of TEMPO-CNFs, which corresponds to the high crystallinity and high moduli of TEMPO-CNFs providing the composite film more superior mechanical properties. The work of fracture of the films showed the highest at 2% TEMPO-CNF containing films. This is evident from the effect of the TEMPO-CNFs. However, with the higher concentration of the TEMPO-CNFs, the decreased strain caused lowering at work of fractures.

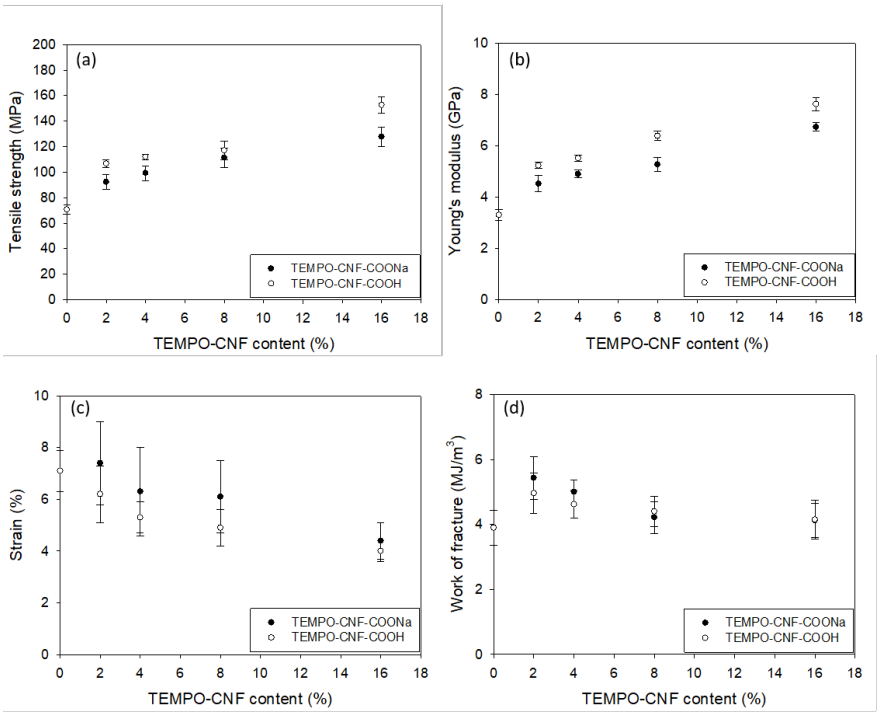

Figure 4.8: The tensile properties plotted against TEMPO-CNF content. a:tensile strength, b:Young's modulus, c: strain, d: work of fracture.

4.5 X-ray Diffractions

The XRD patterns of the films are shown in Fig. 4.9. The broad peaks between 10-30° are characteristic peaks of amorphous cellulose acetate [22, 23]. In the XRD patterns for pure TEMPO-CNF-COONa and TEMPO-CNF-COOH films, two characteristic peaks are present. One at 23° indicates the plane (2 0 0) of cellulose, and another at 15-18° indicates the planes (1 1 0) and (1 -1 0). The TEMPO-CNF peaks gradually becomes more apparent with increasing TEMPO-CNF content.

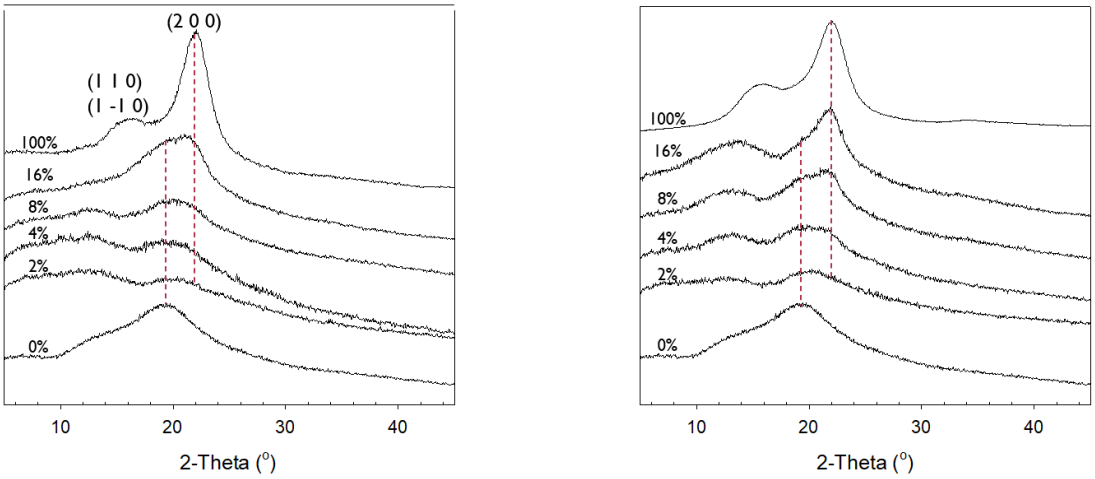

Figure 4.9: The XRD patterns of the films from 0% to 100% TEMPO-CNFs. a: TEMPO-CNF-COONa, b: TEMPO-CNF-COOH.

4.6 Cross-section of the Composite Films

The images of the cross-section for the 16% composite film of both TEMPO-CNFs observed by TEM are shown in Fig. 4.10. These images are used to determine the distribution of TEMPO-CNFs inside the $CA_{DS=0.9}$. The black dots and lines indicate TEMPO-CNFs. In the case of the 16% TEMPO-CNF-COONa composite film, the top surface showed a homogeneous distribution. However, at the bottom of the composite film, a significant amount of clusters are presented compared to the surface. Despite the presence of clusters, a network of TEMPO-CNF-COONa can still be observed, indicating a relatively homogeneous distribution.

For the TEMPO-CNF-COOH, a more homogeneous distribution without a significant amount of clusters is observed. The difference between the two TEMPO-CNFs could be due to the commercial TEMPO-CNF-COONa containing some unfibrillated clusters that remained after production. However, during the conversion to TEMPO-CNF-COOH, the high-pressure homogenizer fibrillated the clusters remained in the commercial TEMPO-CNF-COONa. This process resulted in the TEMPO-CNF-COOH composite films having fewer clusters and more homogenous distribution.

Overall, the TEMPO-CNFs have a homogenous distribution in the $CA_{DS=0.9}$ which provides the composite films with reasonable mechanical properties.

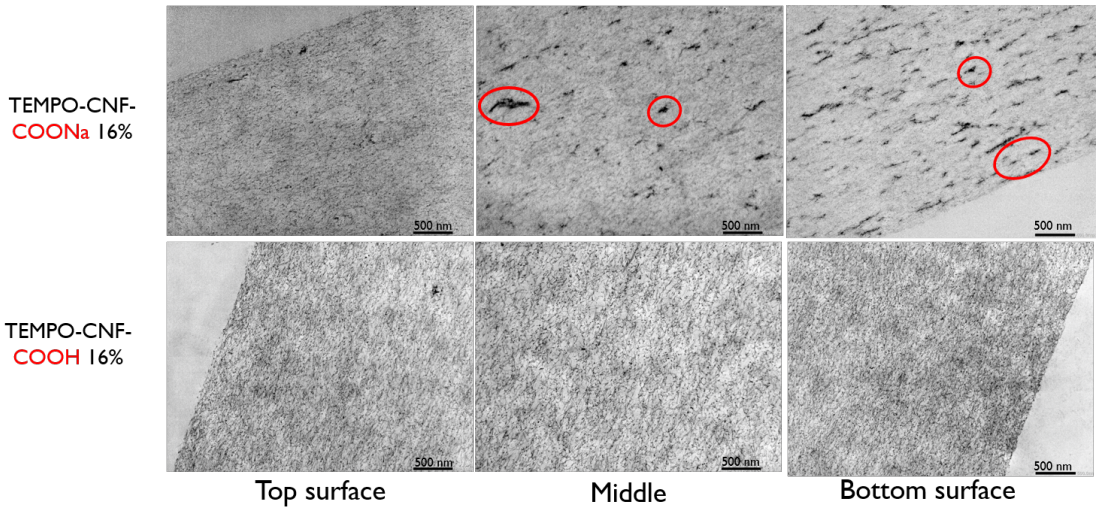

Figure 4.10: The images for the cross-sections of the 16% composite films observed by TEM.

4.7 Termomechanical Analysis

The thermal expansion of the films is shown in Fig. 4.11. The linear lines in the graphs represent the thermal expansion of pure TEMPO-CNF-COONa and TEMPO-CNF-COOH films. The coefficients of thermal expansion (CTE) for the TEMPO-CNF-COONa and TEMPO-CNF-COOH films are 8.27 ppm/°C and 9.92 ppm/°C, respectively. These CTEs are close to that of glass, which is about 9 ppm/°C [19]. The extremely low CTEs are mainly attributed to the high crystallinity of the TEMPO-CNFs.

In the case of the pure $CA_{DS=0.9}$ film, an shrinkage is observed with around 50 to 80°C. However, with increasing TEMPO-CNF content, the shrinkage caused by $CA_{DS=0.9}$ gradually decreases. The CTEs of the composite films could not be calculated due to this shrinkage.

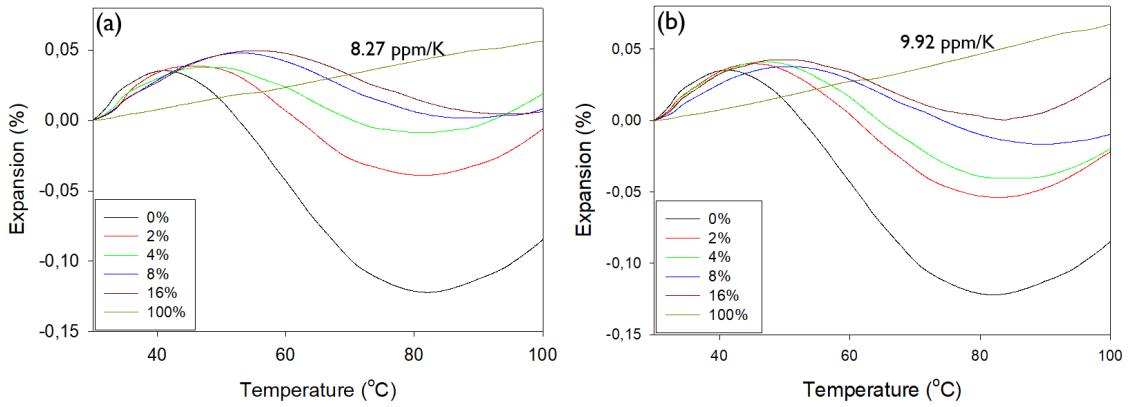

Figure 4.11: The thermal expansions of the films from 0% to 100% TEMPO-CNF. a: TEMPO-CNF-COONa, b: TEMPO-CNF-COOH.

5

Conclusion

In conclusion, TEMPO-CNFs are excellent nanoreinforcements for $CA_{DS=0.9}$ in terms of enhancing tensile properties and maintaining excellent optical properties. The tensile strengths and Young's modulus of the composites showed significant improvement with increasing TEMPO-CNF concentrations. Moreover, the change from TEMPO-CNF-COONa to TEMPO-CNF-COOH further enhanced both of them, indicating a stronger structure of the composite films. The cross-section images obtained using TEM confirmed a homogeneous distribution of TEMPO-CNFs within the films, providing the composite films with reasonable mechanical properties.

The TEMPO-CNFs did not have a negative effect on the composite films, which maintained the high transparency of the $CA_{DS=0.9}$. However, the height differences caused by individual CNF fibrils on the surface of $CA_{DS=0.9}$ at low concentrations of TEMPO-CNFs might have contributed to a high haze value in the composite films. The XRD patterns showed that the crystallinity increased with increasing TEMPO-CNF contents. A difference between the 8% and 16% samples of -COOH and -COONa was also observed, where the -COOH films showed higher crystallinity.

However, some improvements still need to be made to these composite films. One issue is their water resistance, which is caused by the hydrophilic behavior of both $CADS = 0.9$ and TEMPO-CNFs, making the composite films weak to water. Additionally, CA materials are generally considered flammable, low heat resistance, and low chemical resistance. Therefore, if a wider application of the composites is desired, more research still needs to be conducted for these composites.

Bibliography

[1] Saheb, D. N.; Jog, J. P. Natural Fiber Polymer Composites: A Review. *Adv. Polym. Technol.* **1999**, *18* (4), 351–363. https://doi.org/10.1002/(SICI)1098-2329(199924)18:4<351::AID-ADV6>3.0.CO;2-X.

[2] Isogai, A. Emerging Nanocellulose Technologies: Recent Developments. *Adv. Mater.* **2021**, *33* (28), 2000630. https://doi.org/10.1002/adma.202000630.

[3] Yi, T.; Zhao, H.; Mo, Q.; Pan, D.; Liu, Y.; Huang, L.; Xu, H.; Hu, B.; Song, H. From Cellulose to Cellulose Nanofibrils—A Comprehensive Review of the Preparation and Modification of Cellulose Nanofibrils. *Materials* **2020**, *13* (22), 5062. https://doi.org/10.3390/ma13225062.

[4] Fischer, S.; Thümmler, K.; Volkert, B.; Hettrich, K.; Schmidt, I.; Fischer, K. Properties and Applications of Cellulose Acetate. *Macromol. Symp.* **2008**, *262* (1), 89–96. https://doi.org/10.1002/masy.200850210.

[5] Samios, E.; Dart, R. K.; Dawkins, J. V. Preparation, Characterization and Biodegradation Studies on Cellulose Acetates with Varying Degrees of Substitution. *Polymer* **1997**, *38* (12), 3045–3054. https://doi.org/10.1016/S0032-3861(96)00868-3.

[6] Kamide, K.; Saito, M. Thermal Analysis of Cellulose Acetate Solids with Total Degrees of Substitution of 0.49, 1.75, 2.46, and 2.92. *Polym. J.* **1985**, *17* (8), 919–928. https://doi.org/10.1295/polymj.17.919.

[7] Zambrano, F.; Starkey, H.; Wang, Y.; Abbati De Assis, C.; Venditti, R.; Pal, L.; Jameel, H.; Hubbe, M. A.; Rojas, O. J.; Gonzalez, R. Using Micro- and Nanofibrillated Cellulose as a Means to Reduce Weight of Paper Products: A Review. *BioResources* **2020**, *15* (2), 4553–4590. https://doi.org/10.15376/biores.15.2.Zambrano.

[8] Kao Global Chemicals Japan. CNF (Cellulose Nanofiber). https://chemical.kao.com/global/lunaflex/about/cnf/ (accessed March 4, 2024).

[9] Steinmeier, H. 3. Acetate Manufacturing, Process and Technology 3.1 Chemistry of Cellulose Acetylation. *Macromol. Symp.* **2004**, *208* (1), 49–60. https://doi.org/10.1002/masy.200450405.

[10] Malm, C. J.; Tanghe, L. J.; Laird, B. C. Preparation of Cellulose Ac-

etate - Action of Sulfuric Acid. *Ind. Eng. Chem.* **1946**, *38* (1), 77–82. https://doi.org/10.1021/ie50433a033.

[11] Fujisawa, S.; Okita, Y.; Fukuzumi, H.; Saito, T.; Isogai, A. Preparation and Characterization of TEMPO-Oxidized Cellulose Nanofibril Films with Free Carboxyl Groups. *Carbohydr. Polym.* **2011**, *84* (1), 579–583. https://doi.org/10.1016/j.carbpol.2010.12.029.

[12] Okahashi, K.; Takeuchi, M.; Zhou, Y.; Ono, Y.; Fujisawa, S.; Saito, T.; Isogai, A. Nanocellulose-Containing Cellulose Ether Composite Films Prepared from Aqueous Mixtures by Casting and Drying Method. *Cellulose* **2021**, *28* (10), 6373–6387. https://doi.org/10.1007/s10570-021-03897-5.

[13] Hart, E. W. Theory of the Tensile Test. *Acta Metall.* **1967**, *15* (2), 351–355. https://doi.org/10.1016/0001-6160(67)90211-8.

[14] Methods in Lignin Chemistry; Lin, S. Y., Dence, C. W., Eds.; Timell, T. E., Series Ed.; Springer Series in Wood Science; Springer Berlin Heidelberg: Berlin, Heidelberg, **1992**. https://doi.org/10.1007/978-3-642-74065-7.

[15] JASCO International Co., Ltd. Haze Measurement using a UV-Visible Spectrophotometer. https://www.jasco-global.com/solutions/haze-measurement-using-a-uv-visible-spectrophotometer/ (accessed March 4, 2024).

[16] Saba, N.; Jawaid, M. A Review on Thermomechanical Properties of Polymers and Fibers Reinforced Polymer Composites. *J. Ind. Eng. Chem.* **2018**, *67*, 1–11. https://doi.org/10.1016/j.jiec.2018.06.018.

[17] Bunaciu, A. A.; Udriştioiu, E. G.; Aboul-Enein, H. Y. X-Ray Diffraction: Instrumentation and Applications. *Crit. Rev. Anal. Chem.* **2015**, *45* (4), 289–299. https://doi.org/10.1080/10408347.2014.949616.

[18] Wang, Z. L. Transmission Electron Microscopy of Shape-Controlled Nanocrystals and Their Assemblies. *J. Phys. Chem. B* **2000**, *104* (6), 1153–1175. https://doi.org/10.1021/jp993593c.

[19] Fukuzumi, H.; Saito, T.; Iwata, T.; Kumamoto, Y.; Isogai, A. Transparent and High Gas Barrier Films of Cellulose Nanofibers Prepared by TEMPO-Mediated Oxidation. *Biomacromolecules* **2009**, *10* (1), 162–165. https://doi.org/10.1021/bm801065u.

[20] Poyraz, B.; Tozluoğlu, A.; Candan, Z.; Demir, A.; Yavuz, M.; Büyuksarı, Ü.; Ünal, H. İ.; Fidan, H.; Saka, R. C. TEMPO-Treated CNF Composites: Pulp and Matrix Effect. *Fibers Polym.* **2018**, *19* (1), 195–204. https://doi.org/10.1007/s12221-018-7673-y.

[21] Saini, S.; Quinot, D.; Lavoine, N.; Belgacem, M. N.; Bras, J. β-Cyclodextrin-Grafted TEMPO-Oxidized Cellulose Nanofibers for Sustained Release of Essential Oil. *J. Mater. Sci.* **2017**, *52* (7), 3849–3861. https://doi.org/10.1007/s10853-016-0644-7.

[22] Cindradewi, A. W.; Bandi, R.; Park, C.-W.; Park, J.-S.; Lee, E.-A.; Kim, J.-

K.; Kwon, G.-J.; Han, S.-Y.; Lee, S.-H. Preparation and Characterization of Cellulose Acetate Film Reinforced with Cellulose Nanofibril. *Polymers* **2021**, *13* (17), 2990. https://doi.org/10.3390/polym13172990.

[23] Sharma, A.; Mandal, T.; Goswami, S. Fabrication of Cellulose Acetate Nanocomposite Films with Lignocelluosic Nanofiber Filler for Superior Effect on Thermal, Mechanical and Optical Properties. *Nano-Struct. Nano-Objects* **2021**, *25*, 100642. https://doi.org/10.1016/j.nanoso.2020.100642.

DEPARTMENT OF SOME SUBJECT OR TECHNOLOGY
CHALMERS UNIVERSITY OF TECHNOLOGY
Gothenburg, Sweden
www.chalmers.se

CHALMERS
UNIVERSITY OF TECHNOLOGY